BIOLOGICAL CRYSTALLOGRAPHY
ISSN 1399-0047

Structural insights into conformational switching in the copper metalloregulator CsoR from *Streptomyces lividans*

Tatiana V. Porto, Michael A. Hough and Jonathan A. R. Worrall*

School of Biological Sciences, University of Essex, Wivenhoe Park, Colchester CO4 3SQ, England. *Correspondence e-mail: jworrall@essex.ac.uk

Received 22 April 2015
Accepted 6 July 2015

Edited by Q. Hao, University of Hong Kong

Keywords: CsoR; allostery; copper; metalloregulator.

PDB reference: CsoR, 4uig

Supporting information: this article has supporting information at journals.iucr.org/d

Copper-sensitive operon repressors (CsoRs) act to sense cuprous ions and bind them with a high affinity under copper stress in many bacteria. The binding of copper(I) leads to a conformational change in their homotetramer structure, causing disassembly of the operator DNA–CsoR complex and evoking a transcriptional response. Atomic-level structural insight into the conformational switching mechanism between the apo and metal-bound states is lacking. Here, a new X-ray crystal structure of the CsoR from *Streptomyces lividans* is reported and compared with a previously reported *S. lividans* CsoR X-ray structure crystallized under different conditions. Based on evidence from this new X-ray structure, it is revealed that the conformational switching between states centres on a concertina effect at the C-terminal end of each α2 helix in the homotetramer. This drives the Cys104 side chain, a copper(I)-ligating residue, into a position enabling copper(I) coordination and as a result disrupts the α2-helix geometry, leading to a compacting and twisting of the homotetramer structure. Strikingly, the conformational switching induces a redistribution of electrostatic surface potential on the tetrameric DNA-binding face, which in the copper(I)-bound state would no longer favour interaction with the mode of operator DNA binding.

1. Introduction

In bacteria, metalloregulators act to control the expression of genes that enable a rapid response to chronic toxicity or deprivation of biologically essential metal ions (O'Halloran, 1993; Giedroc & Arunkumar, 2007; Ma, Jacobsen *et al.*, 2009; Waldron *et al.*, 2009). This is achieved through high-affinity binding to the regulator of its cognate metal ion, which either inhibits or activates operator DNA binding or enhances transcriptional activation (Ma, Jacobsen *et al.*, 2009). Copper is an essential metal ion in many bacterial organisms and has the capacity to function as a cofactor in enzymes and redox proteins owing to its ability to reversibly access the copper(I) and copper(II) oxidation states. This one-electron redox chemistry is also potentially dangerous to the cell if unchecked. Thus, the bioavailability of copper is tightly regulated in the reducing environment of the bacterial cytosol by homeostasis systems that generally comprise of a metallo-regulator that senses elevated copper(I) levels, a membrane effluxer that exports copper(I) out of the cytosol and a copper(I) chaperone that acts to traffic the metal cargo to the required destination (Tottey *et al.*, 2005; Ma, Jacobsen *et al.*, 2009; Waldron & Robinson, 2009).

The CsoR/RcnR family of bacterial metalloregulators have members which are known to directly respond to copper(I)

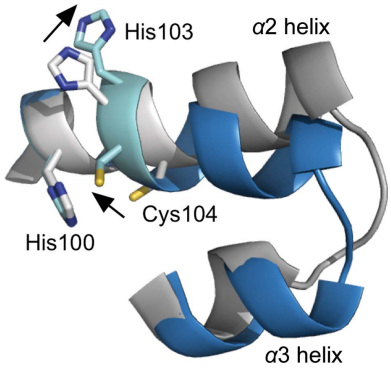

(CsoR; Liu *et al.*, 2007; Smaldone & Helmann, 2007; Ma, Cowart *et al.*, 2009; Sakamoto *et al.*, 2010; Grossoehme *et al.*, 2011; Dwarakanath *et al.*, 2012; Chang *et al.*, 2014), nickel(II)/cobalt(II) (RcnR; Iwig *et al.*, 2006, 2008), nickel(II) (InrS; Foster *et al.*, 2012, 2014) or persulfide (CstR; Grossoehme *et al.*, 2011; Luebke *et al.*, 2014). Bioinformatic analysis has revealed that copper(I)-sensing members of the CsoR/RcnR family are found in four out of seven distinct clades on the basis of sequence identity (Chang *et al.*, 2014). On binding copper(I), CsoR undergoes an allosteric conformational switch that drives negative regulation of DNA binding (Liu *et al.*, 2007). The structures of several copper(I)-regulating CsoRs reveal a protomer consisting of three α-helices of varying lengths arranged in a disc-shaped D_2-symmetric homotetramer (Liu *et al.*, 2007; Sakamoto *et al.*, 2010; Dwarakanath *et al.*, 2012; Chang *et al.*, 2014) that is notable for the absence of a recognizable DNA-binding domain.

Apo CsoR binds to its operator DNA in a 2:1 CsoR tetramer:DNA stoichiometry (Ma, Cowart *et al.*, 2009; Tan *et al.*, 2014). A recent study has presented a plausible model to account for this twofold axis of symmetry, in which each tetrameric face contacts one face of the operator DNA to form a 'sandwich' complex (Tan *et al.*, 2014). How the complex is disassembled or dissociated upon binding copper(I) is not clear. At the molecular level, small-angle X-ray scattering (SAXS) studies using the clade IV *Geobacillus thermodenitrificans* CsoR have indicated a change in the hydrodynamic properties of the copper(I)-bound form to a more compact state, with one dimer within the homotetramer proposed to reorient relative to the other (Chang *et al.*, 2014). These global changes appear subtle but may be of significance for the destabilization or disassembly of the CsoR–DNA complex.

Insights into the conformational switch between the apo and copper(I)-bound states at the atomic level have been inferred through comparison of the copper(I)-bound form of CsoR from one species to that of the apo form from another species owing to the absence of crystal structures for an apo and copper(I) pair from the same species. We report a new X-ray crystal structure of the clade III CsoR from *Streptomyces lividans*. This actinobacterium has a distinct dependence on the bioavailability of copper for morphological development (Fujimoto *et al.*, 2012; Blundell *et al.*, 2013, 2014) and the role of CsoR in copper homeostasis and development has been reported (Dwarakanath *et al.*, 2012; Chaplin *et al.*, 2015). Analysis of the structure reveals it to be in the apo state, but on comparison with our previous *S. lividans* apo CsoR structure (Dwarakanath *et al.*, 2012) significant structural differences throughout the homotetramer assembly are apparent, which based on NMR (Coyne & Giedroc, 2013) and SAXS (Chang *et al.*, 2014) observations of the CsoR from *G. thermodenitrificans* are strongly consistent with features associated with a copper(I)-bound form. We suggest therefore that this new *S. lividans* CsoR X-ray structure may be considered as a 'quasi copper(I)-bound' state. Furthermore, a striking variation in surface-charge distribution between the apo and 'quasi copper(I)-bound' states is revealed that supports a recent report proposing that dissociation of operator DNA is assisted *via* electrostatic occlusion (Chang *et al.*, 2015).

Table 1
Crystallographic data-collection and processing statistics.

Values in parentheses are for the outermost resolution shell.

Wavelength (Å)	0.9163
Resolution (Å)	2.0 (2.05–2.00)
Space group	$I4_122$
Unit-cell parameters (Å)	$a = b = 89.7$, $c = 103.9$
Unique reflections	14603
Completeness (%)	99.7 (99.8)
R_{merge}	0.052 (0.728)
$\langle I/\sigma(I)\rangle$	15.7 (2.3)
Multiplicity	4.9 (4.5)
R_{cryst}	0.211
R_{free}	0.233
E.s.u. based on maximum likelihood (Å)	0.089
R.m.s.d., bond lengths (Å)	0.015
R.m.s.d., bond angles (°)	1.5
Ramachandran favoured (%)	98.9
Wilson *B* factor (Å^2)	27.2
PDB code	4uig

2. Materials and methods

2.1. Crystallization and data collection

Recombinant *S. lividans* CsoR was overexpressed in *Escherichia coli* and purified as described previously (Dwarakanath *et al.*, 2012). Crystals of apo CsoR were initially grown by sitting-drop sparse-matrix screening using an ARI Gryphon crystallization robot. Using the hanging-drop vapour-diffusion method at 20°C, optimization led to single crystals grown from a precipitant solution consisting of 1.8 *M* lithium sulfate, 10 m*M* magnesium sulfate, 50 m*M* sodium cacodylate pH 6. Prior to data collection, a single crystal was transferred to a cryoprotectant solution consisting of 20% glycerol and mother liquor before flash-cooling by plunging into liquid nitrogen. Crystallographic data were measured on beamline I03 at Diamond Light Source using a Pilatus 6M-F detector and an X-ray wavelength of 0.9163 Å.

2.2. Structure determination

Data were processed using *iMosflm* (Battye *et al.*, 2011) and *AIMLESS* (Evans & Murshudov, 2013) in the *CCP*4 suite. The structure was solved by molecular replacement using a single protomer taken from the structure of *S. lividans* apo CsoR (PDB entry 4adz; Dwarakanath *et al.*, 2012) as the search model. The model was refined by maximum-likelihood methods in *REFMAC*5 (Murshudov *et al.*, 2011) and rebuilt between refinement cycles in *Coot* (Emsley & Cowtan, 2004). Riding H atoms were added when refinement of the protein atoms had converged. The model was validated throughout using the *MolProbity* server (Chen *et al.*, 2010) and the *JCSG Quality Control Check* server. Data and refinement statistics together with quality indicators are summarized in Table 1. Structure factors and coordinates have been deposited in the RCSB Protein Data Bank *via* the PDBe, with accession code

4uig. Morph files to reveal the extent of the structural changes between 4adz and 4uig were generated using *CHIMERA* (Pettersen *et al.*, 2004).

3. Results and discussion

3.1. An apo CsoR structure displaying shape similarity to copper(I)-CsoR

X-ray crystal structures have been determined in the copper(I)-bound state for the CsoRs from *Mycobacterium tuberculosis* (Liu *et al.*, 2007) and *G. thermodenitrificans* (Chang *et al.*, 2014) and in the apo state for those from *Thermus thermophilus* HB8 (Sakamoto *et al.*, 2010) and *S. lividans* (Dwarakanath *et al.*, 2012). For crystals of *S. lividans* CsoR grown at pH 6 (in the absence of Cu ions) a tetragonal $I4_122$ space-group symmetry was determined with a single protomer found in the crystallographic asymmetric unit (Table 1). This contrasts with crystals grown at pH 4, which have an orthorhombic $P2_122_1$ space-group symmetry with two protomers located in the asymmetric unit (Dwarakanath *et al.*, 2012). Attempts to crystallize copper(I)-bound CsoR from *S. lividans* using a wide range of crystal screens yielded no diffraction-quality crystals. In the pH 6 protomer structure, well defined electron density was visible from residue 42 up to and including the penultimate residue 132. By applying crystallographic symmetry, the D_2-symmetric homotetramer assembly prevalent in solution was generated (Dwarakanath *et al.*, 2012). As previously described, each tetrameric face utilized to bind operator DNA is essentially dimeric, having two complete monomeric elements (*i.e.* $\alpha1$–$\alpha2$–$\alpha3'$ helices; Dwarakanath *et al.*, 2012). No electron density was visible for residues 1–41, which was also the case in the previously reported pH 4 structure (Dwarakanath *et al.*, 2012) and is indicative of a highly dynamic segment of the CsoR protomer. The N-terminal region of CsoR members is highly variable in sequence and length, with the CsoR from *S. lividans* having one of the longest N-terminal stretches before the start of the core protomer sequence. In the *G. thermodenitrificans* copper(I)-CsoR structure electron density is visible for part of its N-terminal region, revealing it to be folded and lying over the copper(I)-binding site (Chang *et al.*, 2014). The folding of the tail has been considered to be a factor in inhibiting the 2:1 CsoR–DNA assembly (Chang *et al.*, 2014, 2015).

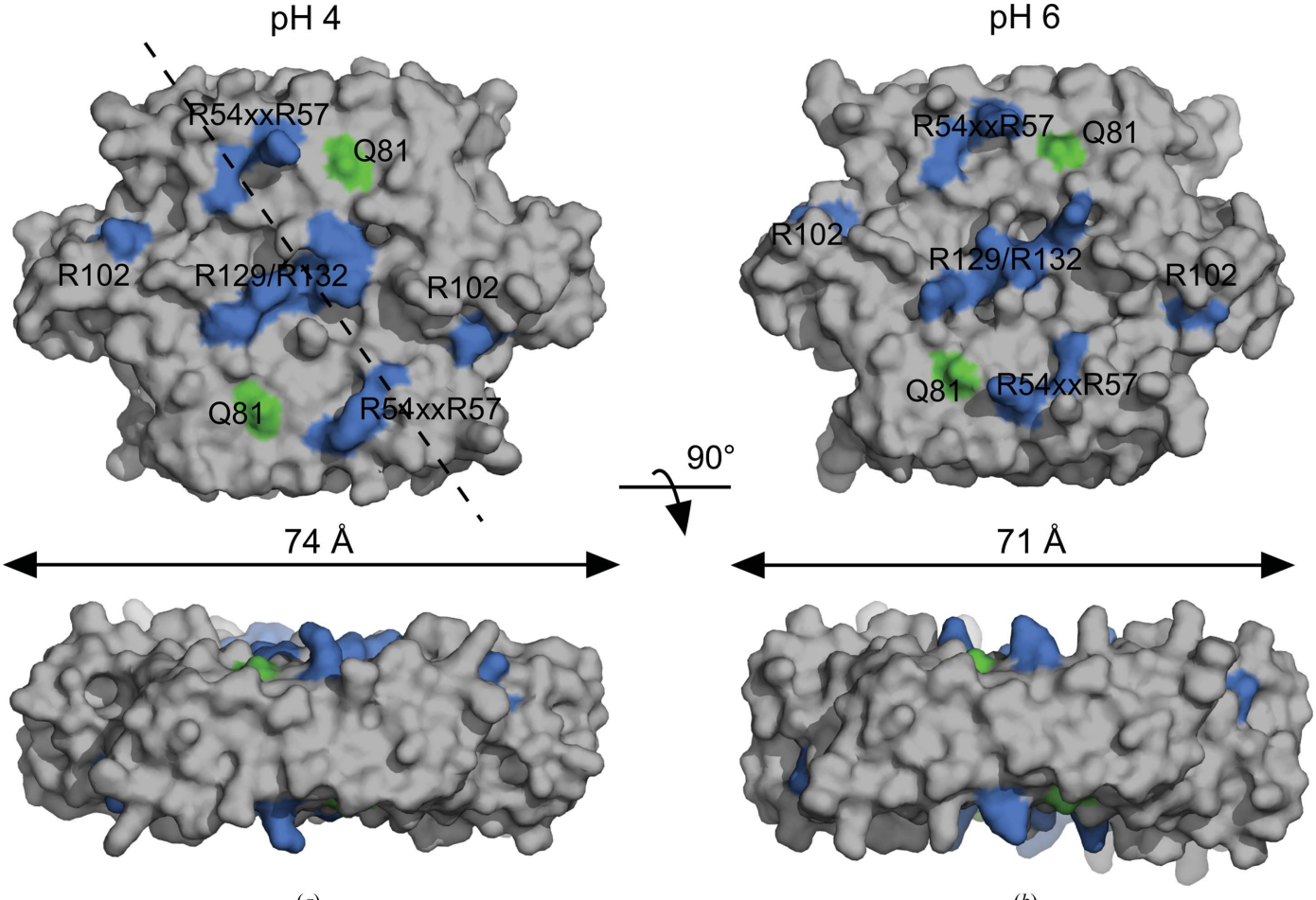

Figure 1
Molecular-surface representations of the homotetramer structure of *S. lividans* CsoR determined from crystals grown at (*a*) pH 4 (PDB entry 4adz; Dwarakanath *et al.*, 2012) and (*b*) pH 6. Residues known or predicted to interact with operator DNA are coloured and labelled on the tetrameric surface. Blue colouring represents positively charged residues and green the polar Gln81. The dashed line indicates the direction in which the operator DNA is predicted to lie on the tetrameric surface (Tan *et al.*, 2014).

Molecular surfaces for the *S. lividans* CsoR X-ray structures at pH 4 (Dwarakanath *et al.*, 2012) and pH 6 are shown in Fig. 1, with residues that are either known (Tan *et al.*, 2014) or suggested (see below) to interact with operator DNA indicated. These form a region on the tetrameric face, with Gln81 as the boundary, whereby the DNA is proposed to lie diagonally within this region in a northwest to southeast direction spanning between the $\alpha1/\alpha1'$ Arg54-*x*-*x*-Arg57 motifs (Chang *et al.*, 2011; Tan *et al.*, 2014; Fig. 1). It is apparent that significant shape differences exist between the two tetrameric structures (Fig. 1). The pH 6 structure displays a clear constriction of the tetrameric face, which is a direct result of the shortening of the axis running along the dimer–dimer interface, decreasing in length from 74 Å in the pH 4 structure to 71 Å in the pH 6 structure (Fig. 1). This constriction also leads to an overall 'swelling' of the homotetramer shape and a seemingly more rugged surface topology of the tetrameric face (bottom panel in Fig. 1). The shape constriction is reminiscent of the differences observed in the calculated scattering envelopes derived from SAXS experiments between the apo and copper(I)-bound states of the CsoR from *G. thermodenitrificans*, with the latter envelope clearly compacted relative to a more elongated apo form (Chang *et al.*, 2014). This hydrodynamic difference was assigned solely to the presence of bound copper(I) (Chang *et al.*, 2014). In fact, Chang and coworkers reveal that the *S. lividans* apo CsoR pH 4 X-ray crystal structure (Dwarakanath *et al.*, 2012) superposes better with the elongated scattering envelope calculated for the apo state of *G. thermodenitrificans* CsoR than does the X-ray crystal structure of the copper(I)-bound form of *G. thermodenitrificans* CsoR (Chang *et al.*, 2014). In the *S. lividans* CsoR pH 6 structure, an electron-density feature consistent with a water molecule (and not consistent with a bound metal ion) was observed between the known copper(I) ligands Cys75′, His100 and Cys104 (Dwarakanath *et al.*, 2012; Fig. 2). The density is consistent with that expected for a water molecule, not an electron-rich metal ion. Thus, the pH 6 homotetramer in the crystal is in an apo state, but with a molecular shape bearing the hallmarks of a copper(I)-bound CsoR in solution (Chang *et al.*, 2014).

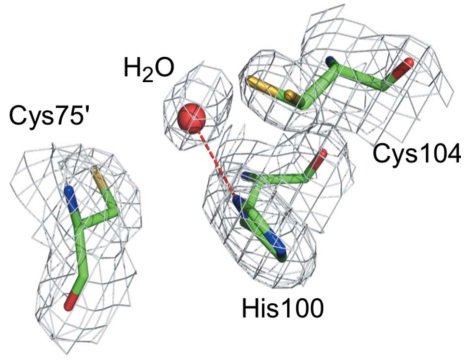

Figure 2
$2F_o - F_c$ electron-density map contoured at 1σ showing the interprotomer copper(I)-binding site in the pH 6 crystal structure of *S. lividans* CsoR. The map reveals the presence of a water molecule hydrogen-bonded to His100 and confirms that no copper(I) is present.

3.2. Rearrangement of the Cys104 side chain disrupts the α2-helical geometry

A secondary-structure-matching superposition of the pH 4 and pH 6 homotetramers reveals a number of features that are associated with compaction of the pH 6 structure. In the pH 4 structure a continuous helical geometry of the $\alpha2$ helices in each protomer is present until residue 112 (Fig. 3*a*). This geometry is clearly disrupted in the pH 6 homotetramer, where the distinctive presence of a 'bulge' or 'kink' in the helix beginning at His103 occurs (Fig. 3*a*). Analysis of NMR chemical shifts have inferred a change in helix geometry

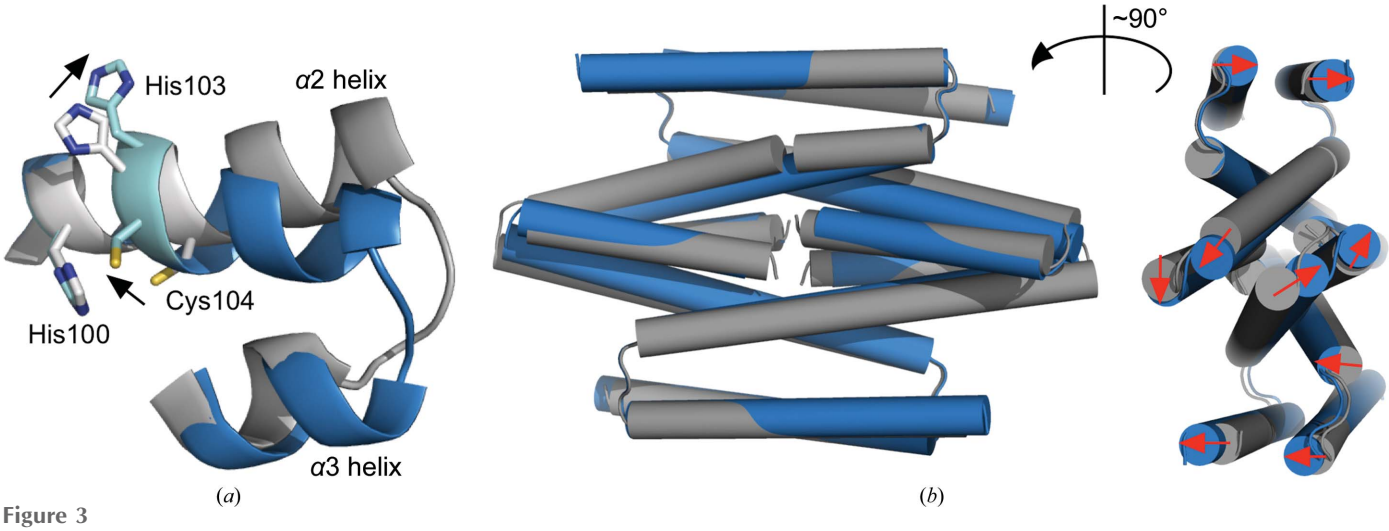

Figure 3
(*a*) Conformational changes at one of the copper(I)-binding sites (grey, pH 4; blue, pH 6) in the *S. lividans* CsoR homotetramer. The creation of the bulge as a result of breaking the helix 2 geometry can be clearly seen and is coloured light blue, with arrows indicating the direction of side-chain movement between states. (*b*) Global structural changes between the pH 4 (grey) and pH 6 (blue) structures. The red arrows indicate the direction of helix movements from pH 4 to pH 6, revealing opposite directionality within each dimer pair.

between the copper(I)-bound and apo states of *G. thermodenitrificans* in the homologous region to *S. lividans* CsoR (Coyne & Giedroc, 2013). Comparison between the *S. lividans* structures indicates that as a consequence of the bulge the side chain of His103 swings outwards and the copper(I) ligand, Cys104, moves upwards into a spatial position that would now enable a metal ion to coordinate to Cys75′, His100 and Cys104 (Fig. 3*a*). This is not the case in the pH 4 structure, where the Cys104 thiol group is not spatially positioned to participate in a first-sphere copper-coordination shell with the other ligands (Fig. 3*a*). Thus, based on the constriction of the homotetramer and the movement of the Cys104 side chain to enable trigonal copper(I) coordination, we suggest that the conformation observed in the crystal at pH 6 can be considered as a 'quasi copper(I)-bound' state.

3.3. Conformational switching involves a concertina effect of the α2 helix

Fig. 3(*b*) shows an overlay of the two *S. lividans* CsoR homotetramers, with arrows to indicate the directionality of the movement in the helices between these conformers. It is apparent from these static overlays that significant helical movement occurs, particularly for the α2 helices between the apo and 'quasi copper(I)-bound' state. These movements are better appreciated through morphing between the two structures (see Supplementary Movies S1 and S2). A concertina effect is observed at the C-terminal ends of the α2 helices creating the bulge/kink, which at the same time causes each dimer in the homotetramer to move in the opposite direction to the other, creating a twist-like motion (Fig. 3*b* and Supplementary Movie S2). These extensive movements, as illustrated in Supplementary Movies S1 and S2, disrupt the surface topology of the tetrameric face and must therefore have consequences for the binding and disassembly of the DNA complex in the respective states.

Operator CsoR DNA sequences consist of a 5′-TAC/GTA-3′ inverted repeat flanking G-tracts of variable lengths (Grossoehme *et al.*, 2011; Dwarakanath *et al.*, 2012; Tan *et al.*, 2014). These poly-d(G) duplexes result in a unique conformation of the DNA that is neither A nor B form, but a B/A hybrid structure. It has previously been demonstrated that the apo state of *S. lividans* CsoR binds operator DNA through a mechanism of conformational selectivity, whereby the binding of two CsoR homotetramers lock the G-tracts into the A conformation (Tan *et al.*, 2014). Based on the flexibility inherent in the homotetramer (Supplementary Movies S1 and S2) and a conformationally selective binding mechanism, we propose that the tetrameric face of the apo state (representative in the pH 4 structure) is structurally optimized to select and stabilize the A conformation of the operator DNA to form a 'sandwich' complex. Upon copper(I) binding (initially to Cys104; T. V. Porto, unpublished data) the conformational switch that occurs pulls copper(I) into full coordination and leads to the bulge/kink in the α2 helices, causing constriction of the homotetramer. This copper(I)-bound state now has a tetrameric face that may no longer be capable of maintaining the operator in the A conformer and leads to the disassembly or disruption of the DNA complex.

3.4. Conformational switching induces an electrostatic redistribution of the tetrameric surface

Whilst the above discussion has offered insight into the global changes that occur on conformational switching between states, the local effects that these changes have on the tetrameric surface (*i.e.* electrostatics) are also likely to influence complex formation and disassembly. A recent study has indicated that electrostatic occlusion may play a role in the copper(I)-induced allosteric switch, whereby residues with significant contacts with the operator DNA in the apo state become 'sequestered' or 'occluded' *via* ion pairing in the copper(I)-bound state, thus leading to reduced operator DNA contact (Chang *et al.*, 2015). These residues have been suggested to be clade-conserved and may be considered as 'regulatory' (Chang *et al.*, 2015). In the clade IV CsoR from *G. thermodenitrificans* a quaternary-structural ion pair that stretches across the tetramer interface (dimer–dimer interface) has been identified in the copper(I)-bound structure, involving side-chain interactions of Glu73 (α2 helix) and Lys101 (α3′ helix) (Chang *et al.*, 2015). A charge-reversal mutation (E73K/K101E) displays DNA-binding properties identical to the wild-type *G. thermodenitrificans* CsoR, strongly suggestive of a key allosteric quaternary-structural interaction critical to maintaining the high-affinity binding in the apo state and/or driving CsoR off the operator DNA when copper(I) is bound (Chang *et al.*, 2015). Moreover, Lys101 is protected from amidination in the DNA-bound and copper(I)-bound states of *Bacillus subtilis* CsoR, indicating that the Lys101 side chain is no longer available for DNA binding and is sequestered (Chang *et al.*, 2011).

In the clade III *S. lividans* CsoR Glu73 is present (Glu98 in *S. lividans* numbering), but a positively charged residue on the α3′ helix in a location that would allow an ion pair is absent. However, a cross-tetramer interface pseudo-ion pair is identified in the pH 6 structure between the N^{ε} atom of Arg102 (α2 helices) and the $O^{\delta1}$ atom of Asp117 (α3′ helices) (Fig. 4*a*). This interaction, together with a hydrogen bond formed between the Arg102 side-chain $N^{\eta1}$ atom and its own backbone carbonyl O atom, ensures that the positively charged guanidino group is orientated in the opposite direction to the DNA-binding face (Figs. 1 and 4*a*). In contrast, the Arg102 guanidino group is no longer sequestered in the apo state (pH 4). This is owing to the reformation of the helical geometry in the α2 helices as opposed to the bulge in the 'quasi copper(I)-bound' state that leads to the reorientation of the Arg102 side chain to point towards the DNA-binding face, therefore favouring a possible interaction with operator DNA. Arg102 has not previously been identified as participating in DNA binding in *S. lividans* CsoR, but its location in the vicinity of the DNA-binding tract on the tetrameric face (Fig. 1) and its switching of side-chain availability between states suggest its involvement. A second notable cross-tetramer interface interaction involving a residue known to interact with DNA in

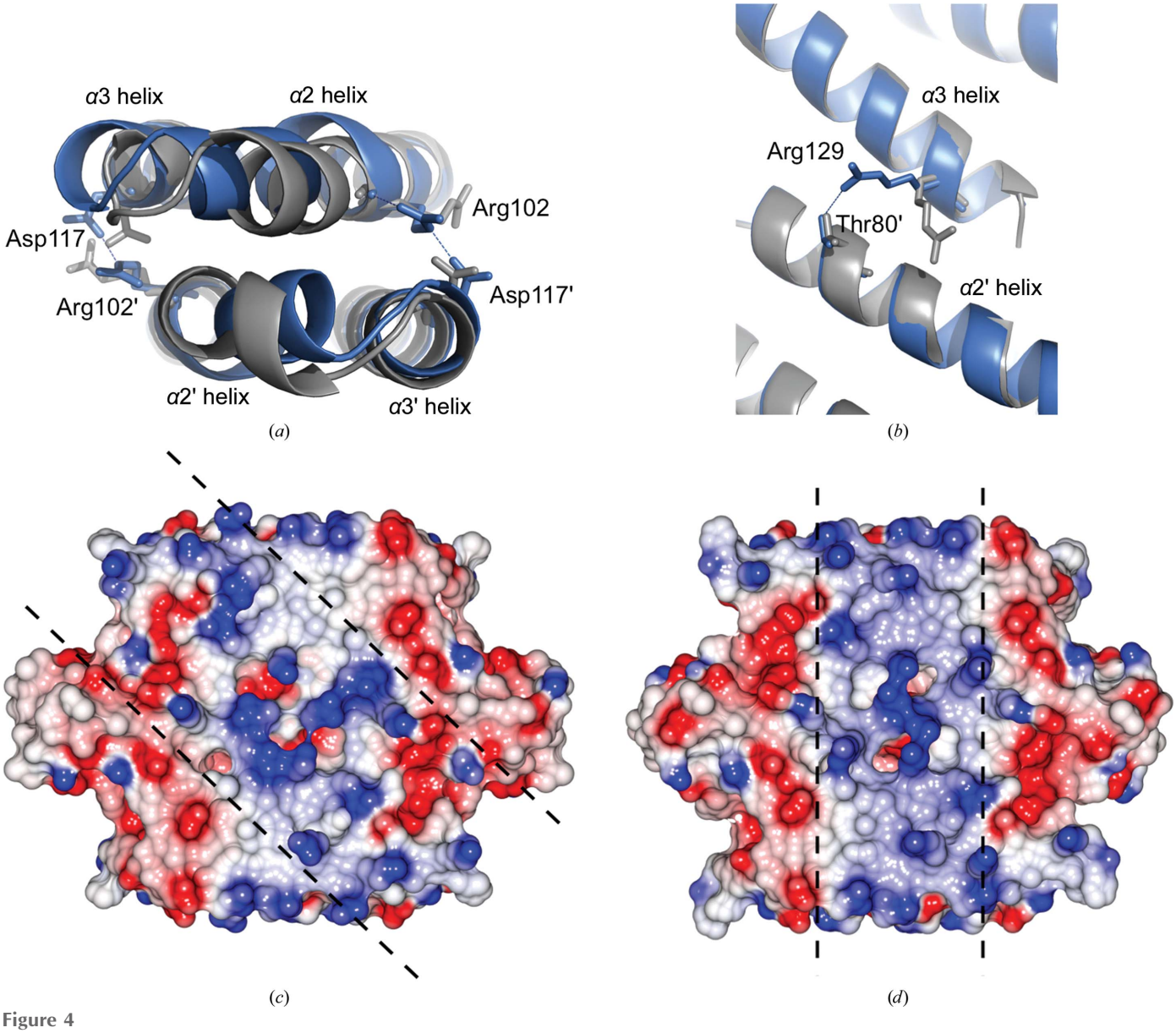

Figure 4
Cross-tetramer interface interactions for (*a*) the Arg102 side chain upon interaction with Asp117 and (*b*) Arg129 and Thr80 (dashed lines) in the quasi copper(I)-bound structure (blue, pH 6). These interactions are absent in the apo state (grey, pH4). Electrostatic surface representations were generated using *CCP4mg* (McNicholas *et al.*, 2011) for the pH 4 (*c*) and pH 6 (*d*) homotetrameric assemblies. Dashed lines in (*c*) indicate the electropositive corridor running northwest to southeast that accommodates operator DNA in the apo state and in (*d*) indicate the redistribution of electropositive charge in a north to south direction.

S. lividans CsoR is identified in the 'quasi copper(I)-bound' structure. This involves the $N^{\eta 1}$ atom of Arg129 and the side-chain $O^{\gamma 1}$ atom of Thr80, an interaction that is absent in the apo structure (pH 4), again caused by the repositioning of the side chain, enabling the guanidino group of Arg129 to interact with the DNA (Tan *et al.*, 2014).

The effect of the above-described local changes and others on switching between states can be further appreciated from the electrostatic potential surfaces of the two homotetramers (Figs. 4*c* and 4*d*). These reveal a striking difference. The electropositively rich corridor running northwest to southeast in the apo state (Fig. 4*c*), which has been experimentally determined to accommodate the operator DNA in the A conformer (Chang *et al.*, 2011; Tan *et al.*, 2014), is abolished in the 'quasi copper(I)-bound' state (Fig. 4*d*). A redistribution of electropositive charge now runs north to south along the homotetramer face, flanked by increased electronegative potential (Fig. 4*d*). Therefore, the structural changes associated with the compaction of the homotetramer lead to a major redistribution of charge (positive and negative) over the tetrameric face that will disrupt the favoured contact with the operator DNA to maintain the A conformer and cause the complex to disassemble.

4. Conclusions

CsoR from *S. lividans* can access different conformational states in crystals grown at different pH values. We propose

that both states observed in the respective crystals are selected through either DNA or copper(I) binding. They should be accessible in solution, but the precise conditions under which they form is hard to predict given the nature of crystallization experiments. The apo state (pH 4) is considered to be conformationally tuned to enable the A conformer of the operator DNA to be stabilized, whereas upon binding copper(I) the pH 6 conformer is favoured. The combination of a change in conformation and the different distribution of surface charge is considered to no longer be optimal for the tetrameric face to keep the bound DNA in the A conformer. This latter observation highlights the importance of comparing different structural states between the same species. Finally, this work indicates that allostery in these disc-shaped tetrameric CsoR proteins, which possess no recognizable DNA-binding domain, is controlled through rather modest structural perturbations that serve to regulate charge redistribution over the tetrameric DNA-binding face.

Acknowledgements

We thank Diamond Light Source for access to beamline I03 (East of England Macromolecular Crystallography BAG, MX9475) that contributed to the results presented here. The use of the *JCSG Quality Control Server* is acknowledged. Morphing was performed with the *UCSF Chimera* package. *Chimera* is developed by the Resource for Biocomputing, Visualization, and Informatics at the University of California, San Francisco (supported by NIGMS P41-GM103311).

References

Battye, T. G. G., Kontogiannis, L., Johnson, O., Powell, H. R. & Leslie, A. G. W. (2011). *Acta Cryst.* D**67**, 271–281.
Blundell, K. L. I. M., Hough, M. A., Vijgenboom, E. & Worrall, J. A. R. (2014). *Biochem. J.* **459**, 525–538.
Blundell, K. L. I. M., Wilson, M. T., Svistunenko, D. A., Vijgenboom, E. & Worrall, J. A. R. (2013). *Open Biol.* **3**, 120163.
Chang, F.-M. J., Coyne, H. J., Cubillas, C., Vinuesa, P., Fang, X., Ma, Z., Ma, D., Helmann, J. D., García-de los Santos, A., Wang, Y.-X., Dann, C. E. & Giedroc, D. P. (2014). *J. Biol. Chem.* **289**, 19204–19217.
Chang, F.-M. J., Lauber, M. A., Running, W. E., Reilly, J. P. & Giedroc, D. P. (2011). *Anal. Chem.* **83**, 9092–9099.
Chang, F.-M. J., Martin, J. E. & Giedroc, D. P. (2015). *Biochemistry*, **54**, 2463–2472.
Chaplin, A. K., Tan, B. G., Vijgenboom, E. & Worrall, J. A. R. (2015). *Metallomics*, **7**, 145–155.
Chen, V. B., Arendall, W. B., Headd, J. J., Keedy, D. A., Immormino, R. M., Kapral, G. J., Murray, L. W., Richardson, J. S. & Richardson, D. C. (2010). *Acta Cryst.* D**66**, 12–21.
Coyne, H. J. & Giedroc, D. P. (2013). *Biomol. NMR Assign.* **7**, 279–283.
Dwarakanath, S., Chaplin, A. K., Hough, M. A., Rigali, S., Vijgenboom, E. & Worrall, J. A. R. (2012). *J. Biol. Chem.* **287**, 17833–17847.
Emsley, P. & Cowtan, K. (2004). *Acta Cryst.* D**60**, 2126–2132.
Evans, P. R. & Murshudov, G. N. (2013). *Acta Cryst.* D**69**, 1204–1214.
Foster, A. W., Patterson, C. J., Pernil, R., Hess, C. R. & Robinson, N. J. (2012). *J. Biol. Chem.* **287**, 12142–12151.
Foster, A. W., Pernil, R., Patterson, C. J. & Robinson, N. J. (2014). *Mol. Microbiol.* **92**, 797–812.
Fujimoto, M., Yamada, A., Kurosawa, J., Kawata, A., Beppu, T., Takano, H. & Ueda, K. (2012). *Microb. Biotechnol.* **5**, 477–488.
Giedroc, D. P. & Arunkumar, A. I. (2007). *Dalton Trans.*, pp. 3107–3120.
Grossoehme, N., Kehl-Fie, T. E., Ma, Z., Adams, K. W., Cowart, D. M., Scott, R. A., Skaar, E. P. & Giedroc, D. P. (2011). *J. Biol. Chem.* **286**, 13522–13531.
Iwig, J. S., Leitch, S., Herbst, R. W., Maroney, M. J. & Chivers, P. T. (2008). *J. Am. Chem. Soc.* **130**, 7592–7606.
Iwig, J. S., Rowe, J. L. & Chivers, P. T. (2006). *Mol. Microbiol.* **62**, 252–262.
Liu, T., Ramesh, A., Ma, Z., Ward, S. K., Zhang, L., George, G. N., Talaat, A. M., Sacchettini, J. C. & Giedroc, D. P. (2007). *Nature Chem. Biol.* **3**, 60–68.
Luebke, J. L., Shen, J., Bruce, K. E., Kehl-Fie, T. E., Peng, H., Skaar, E. P. & Giedroc, D. P. (2014). *Mol. Microbiol.* **94**, 1343–1360.
Ma, Z., Cowart, D. M., Scott, R. A. & Giedroc, D. P. (2009). *Biochemistry*, **48**, 3325–3334.
Ma, Z., Jacobsen, F. E. & Giedroc, D. P. (2009). *Chem. Rev.* **109**, 4644–4681.
McNicholas, S., Potterton, E., Wilson, K. S. & Noble, M. E. M. (2011). *Acta Cryst.* D**67**, 386–394.
Murshudov, G. N., Skubák, P., Lebedev, A. A., Pannu, N. S., Steiner, R. A., Nicholls, R. A., Winn, M. D., Long, F. & Vagin, A. A. (2011). *Acta Cryst.* D**67**, 355–367.
O'Halloran, T. V. (1993). *Science*, **261**, 715–725.
Pettersen, E. F., Goddard, T. D., Huang, C. C., Couch, G. S., Greenblatt, D. M., Meng, E. C. & Ferrin, T. E. (2004). *J. Comput. Chem.* **25**, 1605–1612.
Sakamoto, K., Agari, Y., Agari, K., Kuramitsu, S. & Shinkai, A. (2010). *Microbiology*, **156**, 1993–2005.
Smaldone, G. T. & Helmann, J. D. (2007). *Microbiology*, **153**, 4123–4128.
Tan, B. G., Vijgenboom, E. & Worrall, J. A. R. (2014). *Nucleic Acids Res.* **42**, 1326–1340.
Tottey, S., Harvie, D. R. & Robinson, N. J. (2005). *Acc. Chem. Res.* **38**, 775–783.
Waldron, K. J. & Robinson, N. J. (2009). *Nature Rev. Microbiol.* **7**, 25–35.
Waldron, K. J., Rutherford, J. C., Ford, D. & Robinson, N. J. (2009). *Nature (London)*, **460**, 823–830.